Gravity segregation in steady-state horizontal flow in homogeneous reservoirs

manuscript submitted to *J. Petr. Sci. Eng*.

Gravity Segregation in Steady-State Horizontal Flow in Homogeneous Reservoirs

W. R. Rossen
Department of Petroleum and Geosystems Engineering
The University of Texas at Austin
Austin, TX 78712-1061
U.S.A.
email: wrossen@mail.utexas.edu
fax: 1-512-471-9605
to whom correspondence should be addressed

and
C. J. van Duijn
Department of Mathematics and Computer Science
Eindhoven University of Technology
P. O. Box 513
5600 MB Eindhoven
The Netherlands
email: C.J.v.Duijn@TUE.nl
fax: 31-40-247-2855

Keywords: gravity segregation, gas injection, IOR, gravity override, fractional-flow method, foam

Abstract

The model of Stone and Jenkins for gravity segregation in steady, horizontal gas-liquid flow in homogeneous porous media is extremely useful and apparently general, but without a sound theoretical foundation. We present a proof that this model applies to steady-state gas-liquid flow, and also foam flow. We solve for the lateral position of the point of complete segregation of gas and water flow, but there is still no rigorous solution for the curves separating override, underride and mixed zones, or for the vertical height of the position of complete segregation.

Introduction

Gravity segregation between injected gas and water reduces gas sweep and oil recovery in gas-injection improved oil recovery processes (Lake, 1989). A useful model for gravity segregation is that of Stone (1982) and Jenkins (1984) for steady-state gas-water flow in a homogeneous porous medium. Stone and Jenkins argue that although in the field gas and water are usually injected in alternating slugs, over sufficiently long distances and sufficiently long times the process approximates steady coinjection of the two fluids. Their problem statement begins with the following assumptions:

1. Homogeneous, though possibly anisotropic ($k_v \neq k_h$), porous medium.
2. The reservoir is either rectangular or cylindrical with an open outer boundary. The injection well is completed over the entire vertical interval. The reservoir is confined by no-flow barriers above and below.
3. The system is at steady state, with steady injection of fluids at volumetric rate Q and injected fractional flow of water $f_w = f^J$. This implies that any remaining oil in the region of interest is at its residual saturation and immobile.

Stone and Jenkins then add the standard assumptions of fractional-flow theory for immiscible multiphase flow:

4. Incompressible phases. No mass transfer between phases.
5. Absence of dispersive processes, including fingering, and negligible capillary-pressure gradients.
6. Newtonian mobilities of all phases.
7. Immediate attainment of local steady-state mobilities, which depend only on local saturations.

Assumptions (6) and (7) are clearly valid for gas-water flow, but are more debatable when extending the model to foam flow, as described below. Stone and Jenkins then make the following additional simplifying assumptions:

8. The reservoir splits into three regions of uniform saturation, with sharp boundaries between them, as illustrated in Fig. 1:
   a) an override zone with only gas flowing
   b) an underride zone with only water flowing
   c) a mixed zone with both gas and water flowing
9. At each lateral position x (or r), the pressure gradient in the x (or r) direction is the same in all three regions; i.e., $(\partial/\partial z(\partial p/\partial x)) = 0$. But $\partial p/\partial x$ can (and does) vary with x.

Based on these assumptions, Stone and Jenkins derive equations for the distance L_g (in a rectangular reservoir) or R_g (in a cylindrical reservoir) that the injected gas-water mixture flows before complete segregation, i.e. segregation length, of gas and water flow and for the shape of the boundaries separating the three regions in the reservoir. Shi and Rossen (1998b) show that the equation for a rectangular reservoir can be recast in a way that is useful to the discussion that follows:

$$\frac{L_g}{L} = \frac{1}{N_g R_L} \equiv \left(\frac{(\nabla p)_m}{\Delta \rho g} \right) \left(\frac{H k_h}{L k_v} \right) \tag{1}$$

where L is the length of the reservoir; N_g and R_L are dimensionless gravity number and reservoir aspect ratio, respectively; $(\nabla p)_m$ is the lateral pressure gradient in the mixed zone at the injection face; and $\Delta\rho$ is density difference between phases, g gravitational acceleration, and H reservoir height. For a cylindrical reservoir, the corresponding result is

$$2 = \frac{1}{N_g(R_g) R_L(R_g)} \equiv \left(\frac{\left[(\nabla p)_m (R_g) \right]}{\Delta \rho g} \right) \left(\frac{H k_h}{R_g k_v} \right) . \tag{2}$$

Here gravity number and aspect ratio are defined as functions of the segregation length R_g. Moreover, the pressure gradient used in the gravity number, $[(\nabla p)_m(R_g)]$, is defined as the lateral ∇p that *would* be present in the mixed zone at this radial position R_g in the absence of any gravity segregation. The factor 2 in Eq. (2) derives from the cross-sectional area for flow in a cylindrical domain, i.e. $2\pi r$.

Figure 2 shows a sample prediction of Stone and Jenkins for gas-water flow with the parameter values given in Appendix A. The rock properties and relative-permeability curves are derived from data of Persoff *et al*. (1991) for nitrogen-water flow in Boise sandstone, and viscosities are those of nitrogen and water at room temperature. An interesting feature of this plot is that mobilities are uniform in the three regions but flow rates are not; pressure gradient and volumetric flux in the mixed zone decrease linearly with distance from the well, even in a rectangular reservoir, as shown. The rates of loss of gas to the override zone and of water to the underride zone, in units (volume/time)/(unit length in the lateral direction) are uniform in the mixed zone, unaffected by the decrease in lateral pressure gradient. The boundaries between the zones are not linear, however. As one moves away from the injection face, gas and water leave the mixed zone faster than the zone shrinks in height; hence the total lateral volumetric

flux u_t in the mixed zone decreases, as does lateral pressure gradient, as one moves away from the injection face. At any given value of x, ∇p is the same in all three zones.

The model of Stone and Jenkins fits simulations of gas-water flow over a wide range of parameter values. Still more remarkably, the model fits gravity segregation in simulation of foam injection as well (Shi and Rossen, 1998b), as long as assumptions (1) to (7) hold. The model fits simulation results in spite of the complexity of foam behavior, the extremely large reductions in gas mobility caused by foam, and the abrupt collapse of foam often observed over a narrow range of water saturation (Khatib *et al*., 1988; de Vries and Wit, 1990; Fisher *et al*., 1990; Persoff *et al*., 1991; Rossen and Zhou, 1995; Aronson *et al*., 1994; Alvarez *et al*., 2001). An example is given in Fig. 3. Shi and Rossen (1998b) and Cheng *et al*. (2000) vary injected foam quality, foam strength, foam mechanistic model, flow rates, reservoir dimensions and properties, and even finite-difference grid refinement over a wide range of values with virtually no deviation from predictions of Stone and Jenkins (*cf*. Fig. 4). The model also fits experimental data in a 2D sandpack for gas-water flow (Holt and Vassenden, 1996), and for foam flow as well, if one allows an empirical adjustment to account for an ability of foam to suppress vertical migration in imperfectly homogeneous media (Holt and Vassenden, 1997). "Fit" should be defined carefully in this context. Finite-difference simulations cannot resolve either the vertical or lateral position of complete segregation, H_g or L_g, to better than the size of one grid block. In the simulations, the regions appear remarkably uniform in saturation. The boundaries between regions appear sharp to within one or two grid blocks, as expected in the presence of numerical dispersion. Shi and Rossen (1998b) compare the extent of gravity override qualitatively with the model predictions, while Cheng *et al*. (2000) and Shan (2001) show agreement between model and simulations to within about 4% in L_g (almost to within grid resolution). The value of H_g cannot be compared directly to the simulations because the predicted override zone is usually much thinner than one grid block. It is not clear whether the shape of the boundaries between

regions in simulations has been compared quantitatively to the model; in any case quantitative comparisons would be limited by numerical dispersion and grid resolution at the boundaries; *cf.* Fig. 4.

The implications of Stone and Jenkins' model are profound. Equations (1) and (2) imply that, for a given reservoir and density difference between phases, the only way to increase the distance gas and water travel together before complete gravity segregation is to increase the lateral pressure gradient in the reservoir, at the cost, of course, of increased injection-well pressure. Equivalent improvements are predicted, for instance, from injecting a strong foam at low flow rates, a weak foam at higher rates, or no foam at all at very high rates, to achieve the same value of $(\nabla p)_m$. Moreover, if injection-well pressure is limited, it may be impossible to achieve a desired improvement in vertical sweep. These conclusions, and this paper, however, apply only to continuous-injection foam processes. Shi and Rossen (1998a) and Shan and Rossen (2002) show that alternating-slug foam processes with sufficiently large slugs (larger than those envisioned by Stone and Jenkins) can achieve much better vertical sweep without adversely affecting injection-well pressure.

Uncertain Theoretical Foundation

Thus Stone and Jenkins' model fits a wide range of simulation results and some laboratory data for gas-water flow with or without foam. However, the theoretical justification for the model is uncertain.

Stone (1984) remarks that the process of gravity segregation in 2D flow is similar to gravity segregation in a stagnant porous medium, for which a fractional-flow solution is available (Siddiqui and Lake, 1992); that is, he asserts that the assumptions in his model can be derived from considering an element of fluid spanning the height of the reservoir, moving away from the injection well in time as shown schematically in Fig. 5. It can be seen in two ways that this is not so. First, while a stagnant porous medium is a

closed system, the moving element in Fig. 5 is open. Lateral velocities differ between and vary within the three regions; therefore, for instance, in the override zone gas flows into the element from behind and out its front face with different velocities. Second, gravity segregation in a stagnant medium may feature two shocks, but also one or two spreading waves (*cf.* Fig. 6). Hence one does not always observe two shocks, with uniform regions between, as in Stone and Jenkins' model.

Jenkins (1984) shows a sample fractional-flow function for gravity segregation in a stagnant medium, like Fig. 6, with a shock and a spreading wave, and argues that the average saturations observed in the various zones in 2D flow correspond to the average saturations of any spreading waves predicted from the fractional-flow solution for the stagnant case. This does not explain the observation of two shocks with three uniform regions in the simulations of 2D flow. Moreover, the upper and lower regions in the flow simulations are at their endpoint saturations (or zero saturation of one phase), not at some average saturation of a spreading wave with finite mobility of both phases; *cf.* Fig. 4.

Thus, ironically, a clearly useful model that fits a wide range of simulation results and has important implications for field application is without a firm theoretical justification.

In this paper we prove that a process that obeys assumptions (1) to (7) does indeed spontaneously segregate into three uniform regions with shock fronts between them, and fits Eqs. (1) and (2) for L_g or R_g in rectangular and cylindrical flow, respectively. We are unable to determine the shape of the boundary between the regions apart from their endpoints at the top and bottom of the injection face and their termination at a distance L_g or R_g from the injection face.

Derivation of Equations

The key step in this derivation is the substitution of the stream function ψ for vertical position z in the partial differential equations for flow.

Darcy's law for this system gives, for phase i = water or gas

$$\bar{u}_i = -\lambda_i(S_w)\bar{\bar{k}}(\nabla p + \rho_i g \bar{e}_z) \quad , \tag{3}$$

where $\bar{u}_i$, λ_i and ρ_i are respectively the volumetric flux vector, mobility and density of phase i; $\bar{\bar{k}}$ is the permeability tensor, which we assume has only diagonal elements k_h and k_v, respectively; $\bar{e}_z$ is the unit vector in the vertical direction (pointing upwards). It is also convenient to introduce the reduced water saturation

$$S \equiv \frac{(S_w - S_{wr})}{(1 - S_{wr} - S_{gr})} \quad , \tag{4}$$

where S_{ir} is the residual saturation of phase i.

Mass conservation gives

$$\varphi \frac{\partial S_i}{\partial t} + div(\bar{u}_i) = 0 \quad , \tag{5}$$

with the condition

$$S_w + S_g = 1 \quad . \tag{6}$$

Defining

$$\bar{u}_t = \bar{u}_w + \bar{u}_g \quad , \tag{7}$$

$$\lambda_t(S_w) = \lambda_w(S_w) + \lambda_g(S_w) \quad , \tag{8}$$

it follows that

$$div(\bar{u}_t) = 0 \quad . \tag{9}$$

Combining Eqs. (7), (8) and (3) gives

$$\frac{1}{\lambda_t}\overline{\overline{u}}_t = -\overline{\overline{k}}\nabla p - k_v \frac{\lambda_w \rho_w + \lambda_g \rho_g}{\lambda_t} g \bar{e}_z \quad . \tag{10}$$

Multiplying Eq. (10) by λ_w gives

$$\bar{u}_w = f_w \bar{u}_t - k_v \left(\rho_w - \rho_g\right) g \frac{\lambda_w \lambda_g}{\lambda_t} \bar{e}_z \tag{11}$$

where

$$f_w \equiv \lambda_w / \lambda_t \quad . \tag{12}$$

Equation (9) suggests using the stream function as a basic flow variable. Setting

$$\overline{\overline{u}}_t \equiv \begin{bmatrix} u_{tx} \\ u_{tz} \end{bmatrix} \equiv \begin{bmatrix} -\dfrac{\partial \psi}{\partial z} \\ \dfrac{\partial \psi}{\partial x} \end{bmatrix} \tag{13}$$

we find from Eq. (10)

$$\frac{1}{\lambda_t k_h} \frac{\partial \psi}{\partial z} = \frac{\partial p}{\partial x} \tag{14}$$

$$-\frac{1}{\lambda_t k_v} \frac{\partial \psi}{\partial x} = \frac{\partial p}{\partial z} + \frac{\lambda_w \rho_w + \lambda_g \rho_g}{\lambda_t} g \quad . \tag{15}$$

Differentiating Eqs. (14) and (15) with respect to z and x, respectively, and subtracting the resulting expressions gives the ψ-equation

$$\nabla \bullet \left(\frac{\overline{\overline{T}}}{\lambda_t} \nabla \psi + \frac{\lambda_w \rho_w + \lambda_g \rho_g}{\lambda_t} g \bar{e}_x \right) = 0 \tag{16}$$

where $\bar{e}_x$ is the unit vector in x-direction and where

$$\overline{\overline{T}} \equiv \begin{bmatrix} \frac{1}{k_v} & 0 \\ 0 & \frac{1}{k_h} \end{bmatrix} \quad . \tag{17}$$

At steady state, the water saturation is governed by

$$\nabla \bullet \left(f_w \bar{u}_t - k_v (\rho_w - \rho_g) g \frac{\lambda_w \lambda_g}{\lambda_t} \bar{e}_z \right) = 0 \quad . \tag{18}$$

The corresponding boundary conditions are summarized in Fig. 7.

Both Eqs. (16) and (18) are of the form $\nabla \bullet \overline{G} = 0$. Where $\overline{G}$ is smooth, this equation has its classical interpretation. But across some curve *C* in the *x,z* plane where $\overline{G}$ is discontinuous, the equation has no meaning and should be interpreted in a weak or integrated sense. This implies that

$$\left[\overline{G} \bullet \bar{n} \right] = \{\text{jump of normal component of } \overline{G} \} = 0 \text{ across C} \quad . \tag{19}$$

Applied to Eq. (16), this jump condition becomes

$$\left[\frac{\overline{\overline{T}}}{\lambda_t} \nabla \psi \bullet \bar{n} \right] + \left[\frac{\lambda_w \rho_w + \lambda_g \rho_g}{\lambda_t} \right] g \bar{e}_x \bullet \bar{n} = 0 \quad \text{across C.}$$

Using the definition of ψ and Eq. (10) one observes that Eq. (20) is equivalent to the pressure condition

$$\left[\nabla p \bullet \bar{s} \right] = \{\text{jump of tangent component of p}\} = 0 \quad \text{across C,}$$

implying that the pressure variations on both sides of *C* are identical, i.e., that pressure is continuous across *C*.

Solution for Steady-State Water Saturation

Next we formulate the problem in terms of the water fractional-flow function. Let

$$f \equiv f_w(S_w) \tag{22}$$

and

$$F(S_w) \equiv \frac{\lambda_w(S_w)\lambda_g(S_w)}{\lambda_t(S_w)} = \lambda_g(S_w) f_w(S_w) \ . \tag{23}$$

The monotonicity of $f_w(S_w)$ allows us to consider F as a uniquely defined function of f. Therefore, we also may write $F = F(f)$. Using this and Eq. (9), Eq. (18) becomes

$$\bar{u}_t \bullet \nabla f - k_v(\rho_w - \rho_g) g \frac{\partial}{\partial z} F(f) = 0 \tag{24}$$

The behavior of the function $F = F(f)$ is illustrated in Fig. 8 and discussed further below.

Let us suppose that $u_{tx} > 0$ in the entire flow domain (this has to be verified *a posteriori*). Since $u_{tx} = -\partial\psi/\partial z$, this implies that for any fixed $x > 0$, ψ is strictly decreasing with respect to z. Instead of (x,z), we now take (x, ψ) as independent variables. Writing

$$f = f(x,\psi) = f(x,\psi(x,z)) = f(x,z) \tag{25}$$

we have

$$\left(\frac{\partial f}{\partial x}\right)_z = \left(\frac{\partial f}{\partial x}\right)_\psi + u_{tz}\left(\frac{\partial f}{\partial \psi}\right)_x \ , \tag{26}$$

$$\left(\frac{\partial f}{\partial z}\right)_x = -u_{tx}\left(\frac{\partial f}{\partial \psi}\right)_x \tag{27}$$

and

$$\left(\frac{\partial F(f)}{\partial z}\right)_x = -u_{tx}\left(\frac{\partial F(f)}{\partial \psi}\right)_x \ . \tag{28}$$

Substituting these expressions into Eq. (24) gives the first-order conservation law

$$\left(\frac{\partial f}{\partial x}\right)_{\psi} + k_v(\rho_w - \rho_g)g\left(\frac{\partial F(f)}{\partial \psi}\right)_x = \left(\frac{\partial f}{\partial x}\right)_{\psi} + k_v\ (\rho_w - \rho_g)g\frac{dF}{df}\left(\frac{\partial f}{\partial \psi}\right)_x = 0\ , \quad (29)$$

in the domain $x > 0$, $0 < \psi < Q$.

Equation 29 is in the same form as familiar fractional-flow problems, except that x replaces time and ψ replaces space as independent variables and the displacement depends on the function $F(f)$ rather than $f_w(S_w)$ for 1D displacements (Lake 1989) or $F(S_w)$ for gravity segregation without horizontal flow (Siddiqui and Lake, 1992; *cf*. Fig. 6). Of course both F and f are functions of S_w (or, equivalently, S), but it is $\mathrm{d}F/\mathrm{d}f = (\mathrm{d}F/\mathrm{d}S_w)/(\mathrm{d}f/\mathrm{d}S_w)$ that governs the slope of characteristics.

The solution to Eq. (29) is subject to the boundary condition $f(\psi,0) = f^J$ for $0 < \psi < Q$, which plays the role of the initial condition in conventional fractional-flow problems, and $f(0,x) = 0$, $f(Q,x) = 1$ for all $x > 0$ (*cf*. Fig. 7). That is, the total injection rate Q enters along the injection face, no water flows along the top boundary of the reservoir and no gas flows along the lower boundary. The method of characteristics applied in the ψ,x plane indicates that characteristics with slope $\mathrm{d}F/\mathrm{d}f < 0$ issue from the lower corner of the reservoir, and the slope must decrease monotonically from that at $f = f^J$, the injected fractional flow, to $f = 1$ at the bottom of the reservoir. Similarly, characteristics issue from the top corner with slope $\mathrm{d}F/\mathrm{d}f > 0$ and must have monotonically increasing slope from $f = f^J$ to $f = 0$. Figure 8 shows an example of the function $F(f)$ for the same set of gas-flood parameters as in Figs. 2 and 4. If this function is everywhere concave as shown here, then there are no spreading waves; instead, there are two shock fronts between regions of constant state with values of $f = 0$, f^J and 1. We return to the issue of the shape of the function $F(f)$ below.

The upper shock, separating $f = 0$ and $f = f^J$, is given by

$$\psi = k_v(\rho_w - \rho_g)g\frac{F(f^J)}{f^J}x \quad . \quad (30)$$

The lower shock, separating $f = f^J$ and $f = 1$, is given by

$$\psi = Q - k_v(\rho_w - \rho_g)g\frac{F(f^J)}{(1-f^J)}x \quad . \tag{31}$$

They intersect at the segregation length

$$x = L_g = \frac{Qf^J(1-f^J)}{k_v(\rho_w - \rho_g)gF(f^J)} \quad . \tag{32}$$

Using definition (23), L_g can be rewritten as

$$L_g = \frac{Q}{k_z(\rho_w - \rho_g)g\lambda_t^m} \tag{33}$$

where λ_t^m denotes the total mobility in mixed region. Eq. (33) is the solution for L_g given by Stone (1982); Shi and Rossen (1998b) show that it is equivalent to Eq. (1).

For $x > L_g$, the solution has a shock parallel to the x-axis, separating $f = 0$ and $f = 1$.

The shocks (Eqs. (30) and (31)) are straight lines in (x,ψ) space, but are curves in (x,z) space. Equation 33 gives the exact expression for the x coordinate L_g for the point of complete segregation of flow; Stone and Jenkins also estimate the z coordinate H_g:

$$H_g / H = \left(1 + \frac{1-f^J}{(f^J M_{gw})}\right)^{-1} \tag{34}$$

where M_{gw} is the ratio of gas mobility in the override zone to water mobility in the underride zone. In deriving this expression they assume that all flow is horizontal at the point (L_g,H_g) of complete segregation of liquid and gas. Clearly at some distance downstream of this point this assumption holds and Eq. (34) is valid, but it is doubtful that it applies at $x = L_g$. Although the endpoints of the shock fronts at the corners of the reservoir, and the lateral distance L_g to the point of complete segregation, are known in

(x,z) space, we have no solution for the curved shock fronts themselves. They would result from a free-boundary problem based on Eq. (16). This equation has to be solved in the separate (as yet unknown) subdomains (override, underride, mixed) with Eqs. (20), (30) and (31) as free-boundary conditions. See Appendix B for further discussion.

Segregation distance in cylindrical reservoirs

Let (x,y) denote the horizontal coordinates and $r = \sqrt{x^2 + y^2}$ the distance towards the injection well. Assuming axial-symmetric flow, with

$$\bar{u} = u_r \bar{e}_r + u_z \bar{e}_z, \text{ where } \bar{e}_r = \frac{1}{r}(x, y), \tag{35}$$

the relation between the fluxes and the stream function becomes

$$u_r = -\frac{1}{2\pi r}\frac{\partial \psi}{\partial z}, \quad u_z = \frac{1}{2\pi r}\frac{\partial \psi}{\partial r} \quad . \tag{36}$$

As above, we set

$$f(r,\psi) = f(r,\psi(r,z)) = f(r,z), \tag{37}$$

which results in the equation

$$\frac{1}{2\pi r}\left(\frac{\partial f}{\partial r}\right)_{\psi} + k_v(\rho_w - \rho_g)g\left(\frac{\partial}{\partial \psi}F(f)\right)_r = 0 \tag{38}$$

implying the radial segregation distance

$$R_g = \sqrt{\frac{Q}{\pi k_v (\rho_w - \rho_g) g \lambda_t^m}} \quad . \tag{39}$$

This is the equation for R_g given by Stone (1982); Shi and Rossen (1998b) show that it is equivalent to Eq. (2).

Shape of the Function F(f)

Here we show that only shocks emerge from the corner points ($x = 0,\ \psi = 0$) and ($x = 0,\ \psi = Q$). This follows from the fact that the domain below the function $F(f)$, i.e.

$$D = \{(f,t): 0 \le f \le 1,\ 0 \le t \le F(f)\} \quad , \tag{40}$$

is star-shaped with respect to the points ($f = 0$, $F(0) = 0$), and ($f = 1$, $F(1) = 0$). This property uses only monotonicity of the mobilities $\lambda_g(S)$ and $\lambda_w(S)$.

Let us consider the point ($f = 0$, $F(0) = 0$). Since

$$F(f) = \frac{\lambda_w(S)\lambda_g(S)}{\lambda_t(S)} = f\,\lambda_g(S) \quad , \tag{41}$$

where f and S are related by $f = \lambda_w(S)/\lambda_t(S)$, and since f increases strictly with S, we observe that $\lambda_g(S)$ decreases strictly with f from $\lambda_g(0) > 0$ as $f = 0$ towards $\lambda_g(1) = 0$ as $f = 1$. As a consequence,

$$\lim_{f \downarrow 0} \frac{F(f)}{f} \equiv F'(0) = \lambda_g(0) > 0 \tag{42}$$

and

$$\frac{F(f)}{f} = \lambda_g(S) \tag{43}$$

decreases strictly as f increases (i.e., as S increases). This proves that D is star-shaped with respect to ($f = 0$, $F(0) = 0$) and that a shock is the only solution between $f = 0$ and $f = f^d$.

Similarly, one can write

$$F(f) = (1-f)\lambda_w(S) \quad . \tag{44}$$

Using the monotonicity of $\lambda_w(S)$ we obtain

$$\lim_{f \uparrow 1} \frac{F(f)}{1-f} \equiv -F'(1) = \lambda_w(1) > 0 \tag{45}$$

and ($F(f)/(1-f)$) decreases strictly as f decreases (i.e., as S decreases). Therefore D is also star-shaped with respect to ($f = 1$, $F(1) = 0$) and again a shock is the only solution between $f = f^J$ and $f = 1$.

This proof requires only that $\lambda_w(S)$ be monotically increasing and $\lambda_g(S)$ be monotonically decreasing with S. This property applies to most foam models (Rossen *et al.* 1999; Shi, 1996) as well as more-conventional fluids. The case of foams that obey the "limiting capillary pressure" model (Rossen and Zhou, 1995; Zhou and Rossen, 1995) deserves additional comment. Such a foam collapses abruptly at a limiting water saturation S^*; as a result there are a range of values of λ_g and f, but only one value of λ_w, at S^*. According to Eqs. (43) and (44), the portion of the $F(f)$ curve corresponding to $S = S^*$ lies on a segment that points directly to ($F = 0, f = 1$). Figure 9 shows an example, based on the data of Persoff *et al*. (1991) (Appendix A). Such a case also gives two shocks and regions of uniform state between. More generally, foam may collapse over a narrow range of saturations, rather than at a single value S^*. This sort of behavior is shown in Fig. 10. This behavior likewise gives two shocks and regions of uniform state between.

Conclusions

1. The model of Stone and Jenkins for gravity segregation during steady gas-water co-injection into a homogeneous reservoir is clearly useful and widely applicable; but the theoretical justification given by Stone and Jenkins for their model is not strictly valid, or even self-consistent.
2. In steady incompressible gas-water injection into a rectangular or cylindrical reservoir, at steady state there are three zones of uniform saturation, with sharp boundaries between them: a mixed zone corresponding to the injected

fractional flow, an override zone at irreducible water saturation, and an underride zone with no gas present, as assumed by Stone and Jenkins. This conclusion holds for any two-phase system for which the mobility of the first phase increases monotonically and the mobility of the second phase decreases monotonically as saturation of first phase increases.

3. The distance to the point of complete gravity segregation predicted by theory agrees with that in Stone and Jenkins' model. The three regions are separated by straight-line shock fronts in the (x,ψ) coordinate system. In the conventional (x,z) coordinate system, the shock fronts are curved. Although the lateral distance to the point of complete segregation in the reservoir, and the thickness of the override and underride zones some distance downstream of this point are as given by Stone and Jenkins, the curved shock fronts between the regions are still not determined rigorously.

Acknowledgments

WRR thanks the Centrum voor Wiskunde en Informatica, Amsterdam, for generously supporting his brief sabbatical at which this work was begun. This work was conducted with the support of the Reservoir Engineering Research Program, a consortium of operating and service companies at the Center for Petroleum and Geosystems Engineering at The University of Texas at Austin: Schlumberger Oilfield Services; the Texas Higher Education Coordinating Board's Advanced Technology Program; and the National Petroleum Technology Office of the U. S. Department of Energy, through contracts #DE-AC26-99BC15208 and #DE-AC26-99BC15318. CJvD acknowledges the Institute for Mathematics and Its Applications (IMA) at The University of Minnesota for supporting him while completing this manuscript.

References

Alvarez, J. M., Rivas, H., Rossen, W. R., 2001. A unified model for steady-state foam behavior at high and low foam qualities, SPE J. 6, 325-333..

Aronson, A. S., Bergeron, V., Fagan, M. E., Radke, C. J., 1994. The influence of disjoining pressure on foam stability and flow in porous media, Colloids Surfaces A: Physiochem. Eng. Aspects 83, 109-120.

Cheng, L., Reme, A. B., Shan, D., Coombe, D. A., Rossen, W. R., 2000. Simulating foam processes at high and low foam qualities, SPE 59287, SPE/DOE Symposium on Improved Oil Recovery, Tulsa, OK, 3-5 April.

de Vries, A.S., Wit, K., 1990. Rheology of gas/water foam in the quality range relevant to steam foam, SPE Reservoir Eng. 5, 185-192.

Fisher, A. W., Foulser, R. W. S., Goodyear, S. G., 1990. Mathematical modeling of foam, SPE/DOE 20195, SPE/DOE Symposium on Enhanced Oil Recovery, Tulsa, OK, April 22-24.

Holt, T., Vassenden, F., 1996. Physcial gas/water segregation model. In: S. M. Skjaeveland, S. M. Skauge, A., Hindraker, L., Sisk, C. D. (Ed.): RUTH 1992-1995 Program Summary, Norwegian Petroleum Directorate, Stavanger, 75-84.

Holt, T., Vassenden, T.. 1997. Reduced gas-water segregation by use of foam, 9th European Symposium on Improved Oil Recovery, The Hague, The Netherlands, Oct. 20-22.

Jenkins, M. K., 1984. An analytical model for water/gas miscible displacements, SPE 12632, SPE/DOE 4th Symposium on Enhanced Oil Recovery, Tulsa, OK, April 15-18.

Khatib, Z. I., Hirasaki, G. J., Falls, A. H., 1988 Effects of capillary pressure on coalescence and phase mobilities in foam flowing through porous media, SPE Reservoir Eng. 3, 919-926.

Lake, L., 1989. Enhanced Oil Recovery, Prentice Hall, Englewood Cliffs, NJ.

Persoff, P., Radke, C. J., Pruess, K., Benson, S. M., Witherspoon, P. A., 1991. A laboratory investigation of foam flow in sandstone at elevated pressure, SPE Reservoir Eng. 6, 365-372.

Rossen, W. R., Zeilinger, S. C., Shi, J.-X., Lim, M. T., 1999. Simplified mechanistic simulation of foam processes in porous media, SPE J. 4, 279-287.

Rossen, W. R., Zhou, Z. H., 1995. Modeling foam mobility at the limiting capillary pressure, SPE Adv. Technol. 3, 146-152.

Shan, D., Rossen, W. R.,. 2002. Optimal injection strategies for foam IOR, SPE 75180, SPE/DOE Symposium on Improved Oil Recovery, Tulsa, OK, April 13-17.

Shi, J.-X., Rossen, W. R., 1998a. Improved surfactant-alternating-gas foam process to control gravity override, SPE 39653, SPE/DOE Improved Oil Recovery Symposium, Tulsa, April 19-22.

Shi, J.-X., Rossen, W, R., 1998b. Simulation of gravity override in foam processes in porous media, SPE Reservoir Eval. and Eng. 1, 148-154.

Siddiqui, F. I., Lake, L. W., 1992. A dynamic theory of hydrocarbon migration, Math. Geol. 24, 305-325.

Stone, H. L., 1982. Vertical conformance in an alternating water-miscible gas flood, SPE 11140, 1982 SPE Annual Tech. Conf. and Exhibition, New Orleans, LA, Sept. 26-29.

Zhou, Z. H., Rossen, W. R.,1995. Applying fractional-flow theory to foam processes at the 'limiting capillary pressure', SPE Adv. Technol. 3, 154-162.

Appendix A: Model Parameters Based on Data of Persoff *et al*. (1991)

The gas and water relative-permeability data of Persoff *et al*. (1991) in the absence of foam can be fit by the functions

$$k_{rg} = 0.94\,(1-S)^{1.3} \tag{A1}$$

$$k_{rw} = 0.2\,S^{4.2} \quad . \tag{A2}$$

with $S_{wr} = S_{gr} = 0.2$ (Eq. (4)). We assume $\mu_w = 0.001$ Pa s and $\mu_g = 2 \times 10^{-5}$ Pa s, $\rho_w = 1000$ kg/m^3, $\rho_g = 153$ kg/m^3., which corresponds roughly to N_2 gas at 2000 psi and 300K. In Figs. 2 and 8 we assume that the injected water fractional flow f^I is 0.2.

The equations of Stone and Jenkins use two factors computed from these parameters: M_{gm} is the ratio of the mobility of gas in the mixed zone to the mobility of gas in the override zone, and M_{gw} is ratio of the mobility of gas in the override zone to the mobility of water in the underrride zone. The override zone is at $S_w = S_{wr} = 0.2$; the underride zone is at $S_w = 1$ ($S = 1$), with $k_{rw} = 1$, since it is assumed gas has never entered there. To calculate the mobilities in the mixed zone it is necessary to calculate S_w there from the injected fractional flow f_w:

$$f_w = 0.2 = \frac{1}{1 + \dfrac{k_{rg}(S_w)}{\mu_g}\dfrac{\mu_w}{k_{rw}(S_w)}} \tag{A4}$$

which leads to $S_w = 0.777$, $M_{gm} = 69.24$, and $M_{gw} = 47$.

Both gas relative permeability and viscosity are altered by foam, but for simplicity here we account for all effects for foam by altering the gas relative permeability (Rossen *et al*., 1999). The data of Persoff *et al*. in the presence of foam are fit by retaining the functions above for $S_w < 0.37$. For $S_w > 0.37$, k_{rg} is reduced by a factor of 18,500 (Zhou and Rossen, 1995). For $S_w = 0.37$, k_{rg} is not a unique function of S_w, but must be determined from f_w. For instance, for injected $f_w = 0.2$, $S_w = 0.37$ and (*cf*. Eq. (A4))

$$f_w = 0.2 = \frac{1}{1 + \dfrac{k_{rg}(S_w)}{2\cdot 10^{-5}}\dfrac{10^{-3}}{10^{-3}}} \tag{A5}$$

which gives $k_{rg} = 8\cdot 10^{-5}$, $M_{gw} = 47$ and $M_{gm} = 11750$.

Appendix B: Free-Boundary Problem

The curves separating the phases in the reservoir (in the original x,z coordinates) are determined by the solution of the stream-function equation (Eq. (16)) subject to Eqs. (20), (30) and (31) across the *a priori*-unknown phase boundaries. This is a free-boundary problem which we pose here for completeness.

We begin with a non-dimensionalization and some notation. Setting

$$x := x/H,\ z = z/H \text{ and } L_g^* = L_g/H \ , \tag{B1}$$

let

$$\Omega = \{(x,z) : 0 < \infty,\ 0 < z < 1\} \tag{B2}$$

denote the semi-infinite scaled reservoir in which we identify the regions of mixed flow (Ω_m) and the gas override (Ω_g) and water underride zones (Ω_w) as in Fig. B1. The corresponding phase boundaries are denoted by C_{mg}, C_{mw} and C_{gw}. We assume that they have the horizontal parameterizations

$$C_{mg} = \{(x,z) : 0 \le x \le L_g^*,\ z = h_{mg}(x)\} \ , \tag{B3}$$

$$C_{mw} = \{(x,z) : 0 \le x \le L_g^*,\ z = h_{mw}(x)\} \ , \tag{B4}$$

$$C_{gw} = \{(x,z) : L_g^* \le x \le \infty,\ z = h_{gw}(x)\} \ . \tag{B5}$$

Next we set

$$\alpha := f' \tag{B6}$$

$$\gamma_w := \frac{\rho_w}{\alpha\rho_w + (1-\alpha)\rho_g} \ , \quad K_w := \frac{\lambda_t^m}{\lambda_t^w} \tag{B7}$$

$$\gamma_g := \frac{\rho_g}{\alpha\rho_w + (1-\alpha)\rho_g} \ , \quad K_g := \frac{\lambda_t^m}{\lambda_t^g} \tag{B7}$$

and we nondimensionalize ψ and Q according to

$$(\psi,Q) = (\psi,Q) / H\ \lambda_t^m\ k_v\ (\alpha\rho_w + (1-\alpha)\rho_g)\ g \quad . \tag{B8}$$

Then for ψ results the equation

$$\nabla\bullet(K\ \overline{\overline{T}}\ \nabla\psi + \gamma\ \bar{e}_x) = 0 \ \text{ in } \Omega \tag{B9}$$

where

$$\overline{\overline{T}} = \begin{pmatrix} 1 & 0 \\ 0 & \dfrac{k_v}{k_h} \end{pmatrix} \tag{B10}$$

and where

$$K = \begin{cases} 1\ in\ \Omega_m \\ K_w\ in\ \Omega_w \\ K_g\ in\ \Omega_g \end{cases} \qquad \gamma = \begin{cases} 1\ in\ \Omega_m \\ \gamma_w\ in\ \Omega_w \\ \gamma_g\ in\ \Omega_g \end{cases} \tag{B11}$$

The boundary conditions for ψ are

$$\text{(BC)} \begin{cases} \psi(x,0) = Q, \quad \psi(x,1) = 0 & for\ \ 0 \le x \le \infty \\ \psi(0,z) = Q(1-z), & for\ \ 0 \le x \le \infty \end{cases} \tag{B12}$$

and the values along the phase boundaries

$$\psi|_{C_{mg}} = (1 - \alpha)\ (\gamma_w - \gamma_g)\ x \qquad \text{for } 0 \le x \le L_g^* \tag{B13}$$

$$\psi|_{C_{mw}} = Q - \alpha\ (\gamma_w - \gamma_g)\ x \qquad \text{for } 0 \le x \le L_g^* \tag{B14}$$

$$\psi|_{C_{gw}} = (1 - \alpha)\ Q \qquad \text{for } L_g^* \le x < \infty \tag{B15}$$

where

$$L_g^* = Q / (\gamma_w - \gamma_g) \quad . \tag{B16}$$

The free-boundary problem now reads: Given $0 < \alpha < 1$, $0 < \rho_g < \rho_w$ (specifying γ_g and γ_w), $Q > 0$ and K_w, $K_g > 0$, find ψ: $\overline{\Omega} \rightarrow$ R satisfying

$$\psi \in H^2_{loc}(\Omega) \cap L^\infty(\Omega) \cap C(\overline{\Omega}) \tag{B17}$$

and find

$$h_{mg}, h_{mw} : [0, L_g^*] \rightarrow [0,1] \tag{B18}$$

$$h_{gw} : [L_g^*, \infty) \rightarrow [0,1] \tag{B18}$$

satisfying

$$h_{mw}(x) < h_{mg}(x) \quad \text{for } 0 \le x < L_g^* \tag{B19}$$

and

$$h_{mw}(L_g^*) = h_{mg}(L_g^*) = h_{gw}(L_g^*) \tag{B20}$$

such that

i) Eq. (B9) is satisfied weakly in Ω (B21)

ii) ψ satisfies boundary conditions (B12) (B22)

iii) ψ satisfies Eqs. (B13) to (B15) along the phase boundaries . (B23)

Note that the free-boundary conditions do not involve the parameters K_w and K_g; however, the location of the free boundaries will strongly depend on their values. This is illustrated in Fig. 2, where $K_w = 0.68$, $K_g = 0.014$, and in Fig. 3, where $K_w = 4 \cdot 10^{-3}$, $K_g = 8.5 \cdot 10^{-5}$.

List of Figures

Figure 9. F(f) function for mobility functions of Persoff *et al*. (1991) (Appendix A), where gas mobility decreases abruptly for $S_w > S_w^* = 0.37$ ($S^* = 0.283$). The portion of the curve for $S < S^*$ matches that in Fig. 9 (note change of scale).

Figure 10. Schematic of F(f) for more general foam behavior, where foam collapses over a small range of values of S near S*; *cf*. Fig. 9. Note points on curve for S near S* fall on fan of lines originating at (1,0).

Figure B1. Schematic of regions and boundaries between them in free-boundary problem.

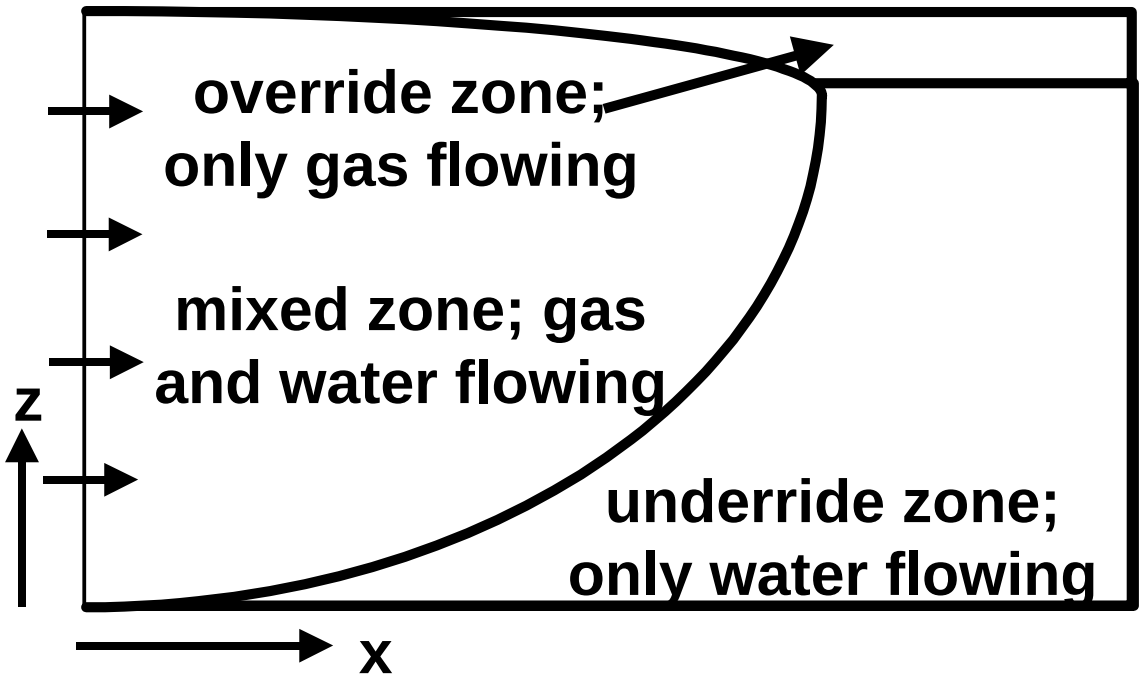

Figure 1. Schematic of three uniform zones in model of Stone and Jenkins.

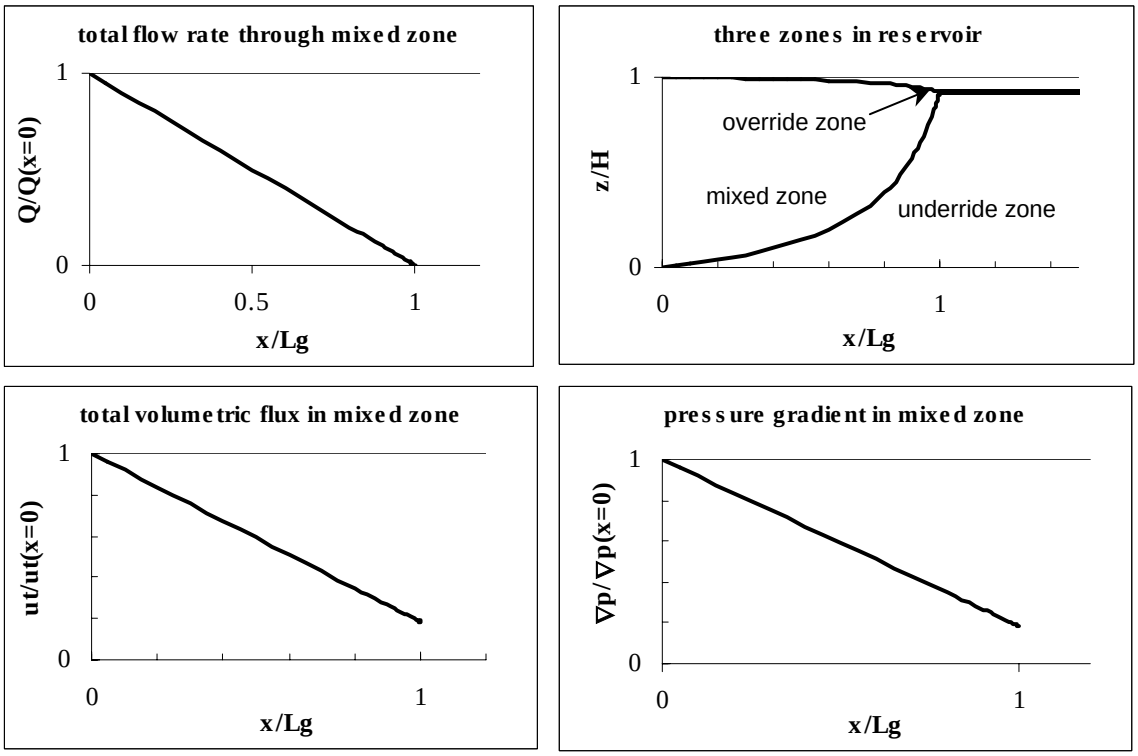

Figure 2. Predictions of model of Stone and Jenkins for gas-water flow without foam. Parameter values are based on data of Persoff *et al*. (1991) for N_2-water flow in Boise sandstone (*cf.* Appendix A).

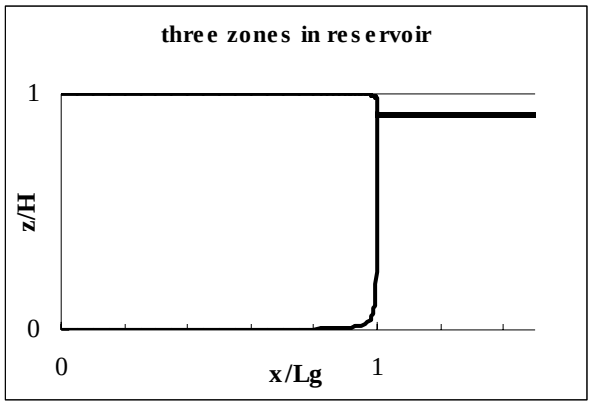

Figure 3. Example of three zones in reservoir predicted by model of Stone and Jenkins for foam injection using parameters based on data of Persoff *et al*. (1991); *cf*. Appendix A.

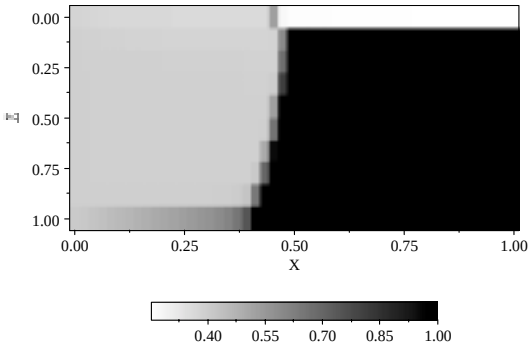

Figure 4. Example of gravity segregation in finite-difference simulation of continuous foam injection into rectangular reservoir, from Shan (2001). Gray scale indicates water saturation: white = override zone, gray = mixed (foam) zone, black = underride zone. In this case complete gravity segregation occurs at $L_g \approx 0.5$. The foam model used here is not identical to that in Fig. 3.

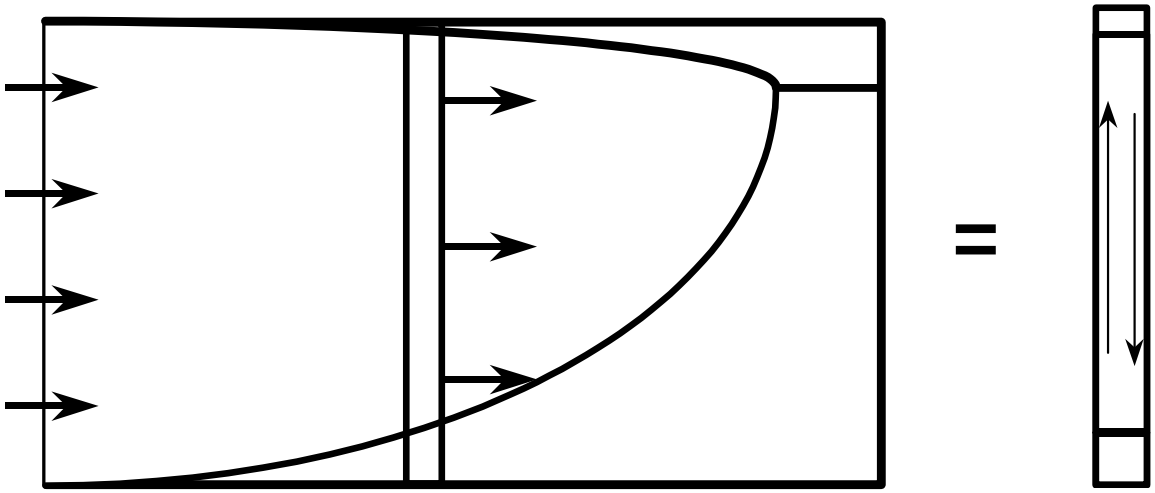

Figure 5. Schematic of assumption of Stone (1982) that a moving vertical fluid element within reservoir maps segregation problem in horizontal flow on to segregation problem without horizontal flow.

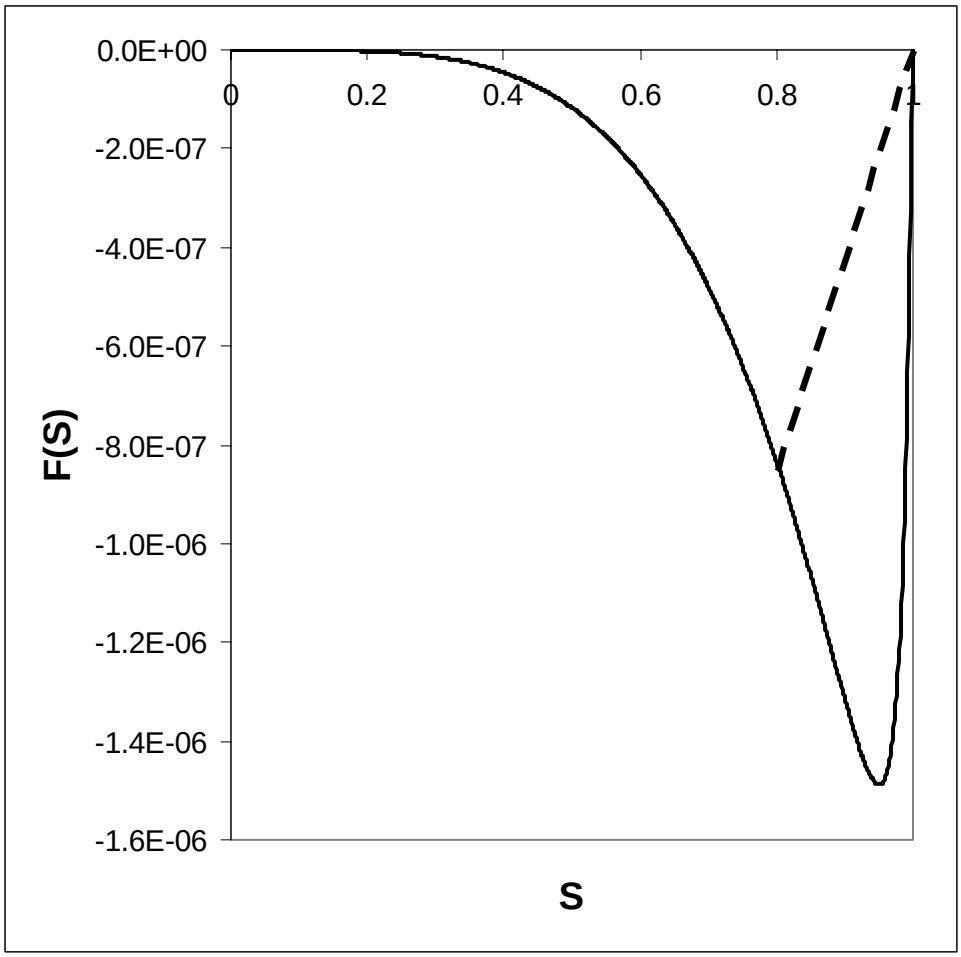

Figure 6. Function $F(S)$ that governs gravity segregation without horizontal flow (Siddiqui and Lake, 1992). Parameters values are those for N_2 and water from Persoff *et al*.(*cf.* Appendix A). If reservoir is initially at $S = 0.8$ (water saturation $S_w = 0.68$), there is a shock front moving from the bottom of the reservoir, which has saturation $S = 1$ ($S_w = .8$) (dotted line), but a spreading wave moving down from the top at $S = 0$ ($S_w = 0.2$).

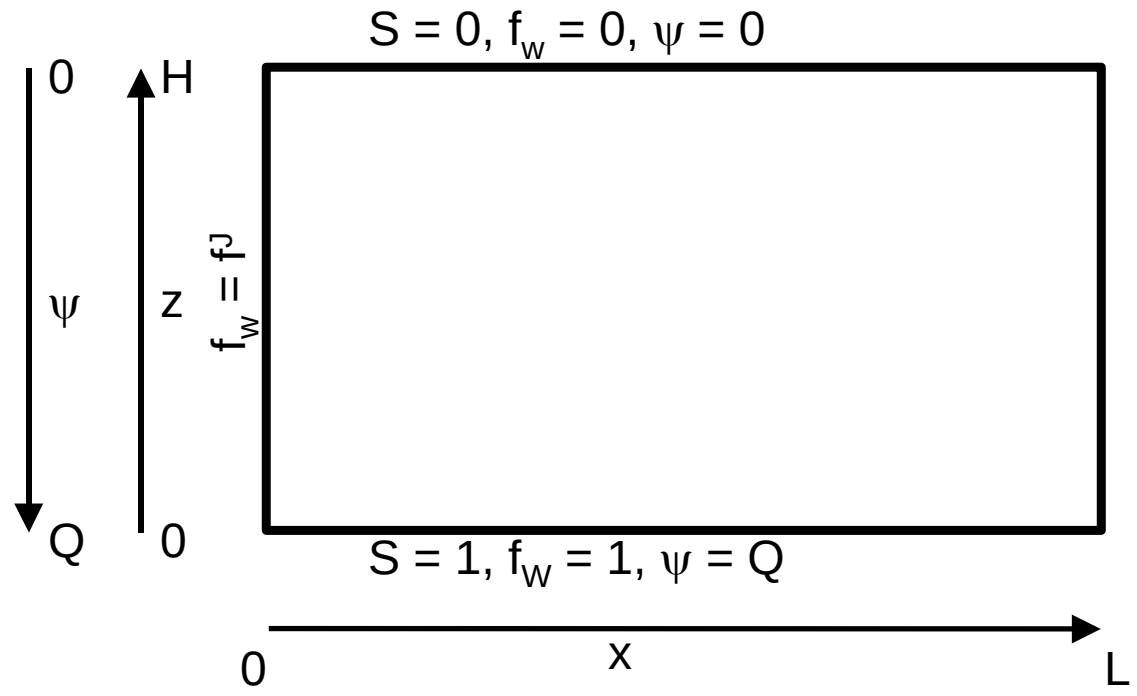

Figure 7. Schematic of boundary conditions in terms of *x* and either *z* or ψ.

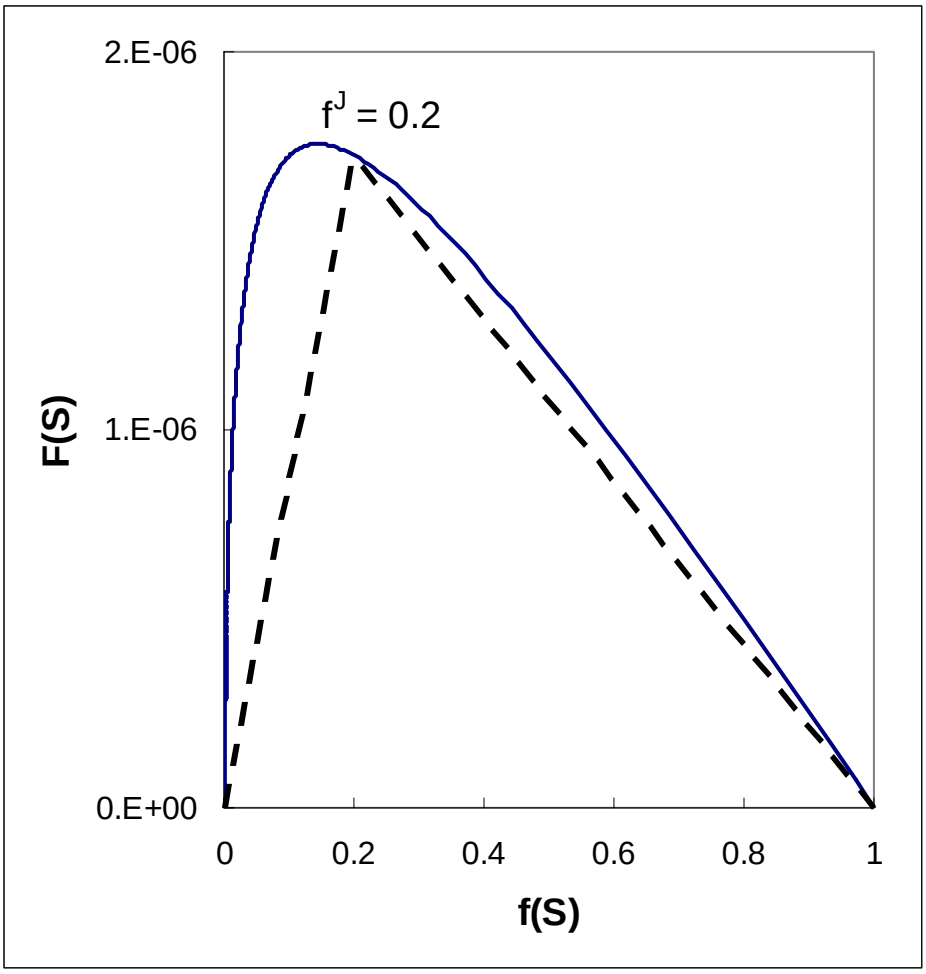

Figure 8. Function F(f) that governs gravity segregation in horizontal flow for N_2 and water. Parameters values are from Persoff *et al*. (1991) (Appendix A). Dotted lines indicate shock fronts between mixed zone ($f = f^J$) and top of reservoir ($f = 0$) and bottom of reservoir ($f = 1$) for foam injected at $f^J = 0.2$.

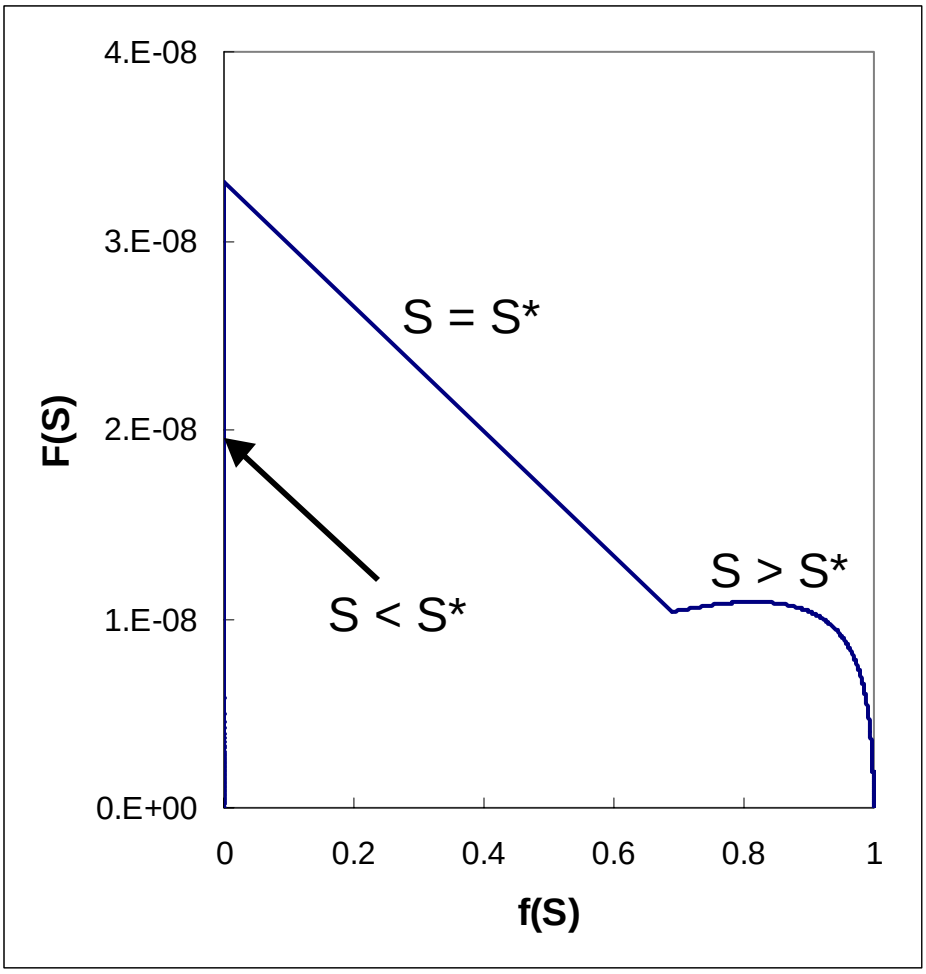

Figure 9. F(f) function for mobility functions of Persoff *et al*. (1991) (Appendix A), where gas mobility changes abruptly at $S_w = S_w* = 0.37$ ($S* = 0.283$). The portion of the curve for $S < S*$ matches that in Fig. 8 (note change of scale).

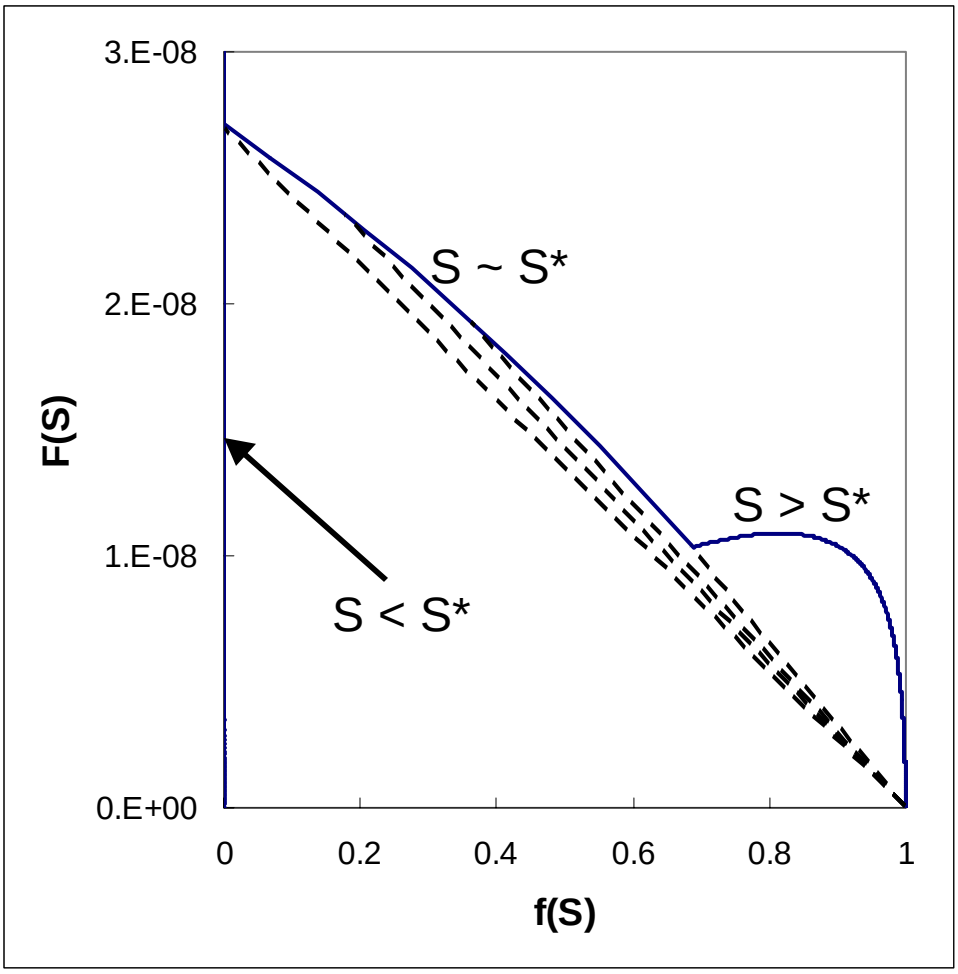

Figure 10. Schematic of $F(f)$ for more general foam behavior, where foam collapses over a small range of values of S near S^*; *cf.* Fig. 9. Note points on curve for S near S^* fall on fan of lines originating at (1,0).

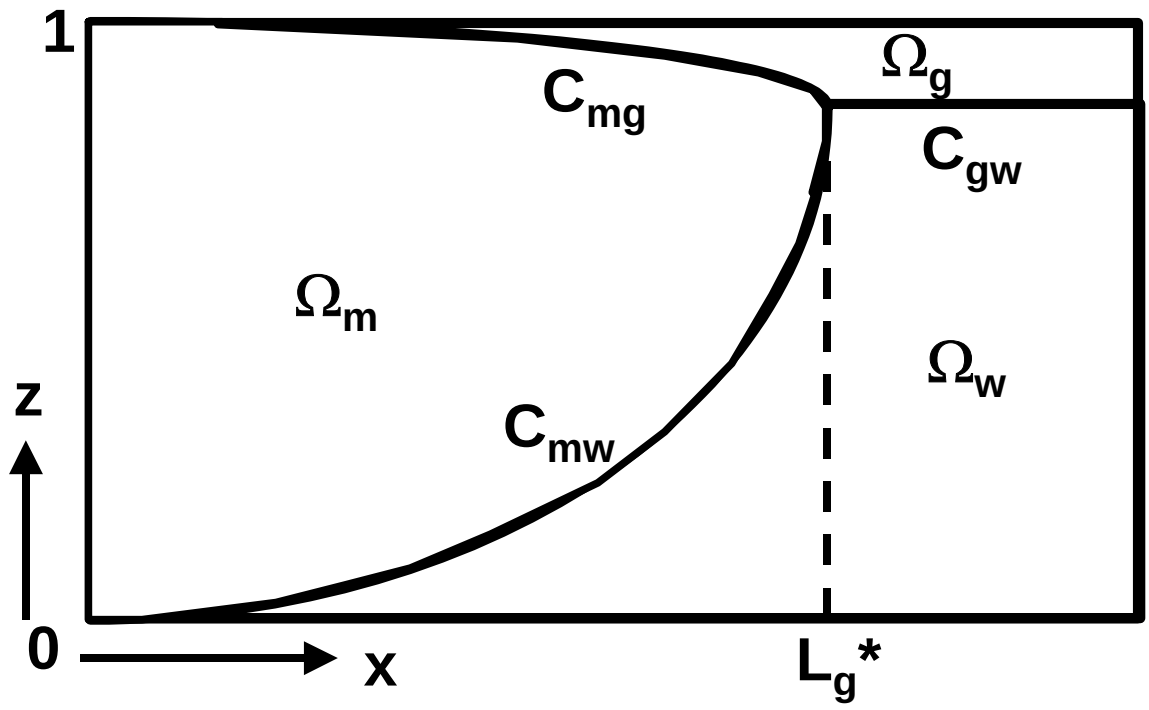

Figure B1. Schematic of regions and boundaries between them in free-boundary problem.